RARE METALS

ORIGINAL ARTICLE

Improvement in antibacterial ability and cell cytotoxicity of Ti–Cu alloy by anodic oxidation

Shuang Cao, Zi-Ming Zhang, Jia-Qi Zhang, Ren-Xian Wang, Xiao-Yan Wang, Lei Yang, Da-Fu Chen*, Gao-Wu Qin, Er-Lin Zhang*

Abstract Ti–Cu alloy has potential to be used in plastic surgery and dental implants due to its strong antibacterial properties, high strength and good corrosion resistance. In this paper, Ti–5Cu was anodic-oxidized to enhance the surface compatibility. The influence of the oxidation on the corrosion resistance, antibacterial properties and biological properties was investigated. X-ray diffraction (XRD) and X-ray photoelectron spectroscopy (XPS) results showed that a double-layer oxide coating with dense inner layer and porous outside layer was formed on Ti–Cu sample. The oxide coating consisted mainly of TiO_2, Cu_2O and small amount of CuO, improved the corrosion resistance of Ti–Cu alloy by one order of magnitude due to the formation of the dense oxide inner layer, but high Cu ion release was detected. The plate count results showed that the antibacterial activity of Ti–Cu sample was improved to $\geq 99\%$ due to the comprehensive function of CuO and Cu_2O in the coating and Cu^{2+} release. Cell test results showed that the coating exhibited good cell compatibility, the porous surface structure improved the adhesion of cells, and Cu ion release promoted the cell proliferation.

Keywords Titanium–copper alloy; Anodic oxidation; Corrosion resistance; Antibacterial activity; Cell adhesion; Surface modification

S. Cao, Z.-M. Zhang, L. Yang, G.-W. Qin, E.-L. Zhang*
School of Materials Science and Engineering, Key Laboratory for Anisotropy and Texture of Materials, Education Ministry of China, Northeastern University, Shenyang 110819, China
e-mail: zhangel@atm.neu.edu.cn

J.-Q. Zhang
Departments of Immunology, College of Basic Medicine, Jiamusi University, Jiamusi 154007, China

R.-X. Wang, D.-F. Chen*
Laboratory of Bone Tissue Engineering, Beijing Laboratory of Biomedical Materials, Beijing Research Institute of Orthopaedics and Traumatology, Beijing Jishuitan Hospital, Beijing 100035, China
e-mail: chendafu@jsthospital.org

X.-Y. Wang
School of Metallurgy, Northeastern University, Shenyang 110819, China

L. Yang, G.-W. Qin, E.-L. Zhang
Research Center for Metallic Wires, Northeastern University, Shenyang 110819, China

1 Introduction

In recent years, titanium (Ti) and its alloys have been widely used in medical implants due to the excellent biocompatibility and mechanical properties [1–8]. However, titanium alloys as biologically inert material have no antibacterial properties, and bacteria easily adhere to the neck of the implant, causing diseases around the implant [9]. When peri-implantitis occurs, high dose of antibiotics must be used for treatment, which not only brings huge pain and economic burden to the patient, but also increases the risk of bacterial resistance. Therefore, it is of great significance to make titanium implants have comprehensive long-term antibacterial properties and improve the ability of early osseointegration [10, 11].

Copper (Cu) promotes the differentiation of osteoblasts and induces angiogenesis. At the same time, as an essential trace element for the human body, it plays a role in preventing osteoporosis [12]. Shirai et al. [13] reported for the first time that a titanium–copper alloy containing 1 wt% or 5 wt% copper prevented needle tract infections. The

in vitro and in vivo experimental results showed that Ti–1 wt% Cu and Ti–5 wt% Cu alloys both had antibacterial effects. Zhang et al. [14] prepared the antibacterial Ti–Cu sintered alloy through powder metallurgy technology, and Ti–Cu sintered alloy showed an antibacterial rate of >99% against *Escherichia coli* (*E. coli*) and *Staphylococcus aureus* (*S. aureus*). However, the stability of antibacterial ability is good when the copper content is > 5 wt%. Liu et al.'s in vitro and in vivo experiments confirmed that Ti–5Cu alloy had excellent antibacterial properties, biocompatibility and bone formation [5]. It has been shown that the addition of Cu to Ti alloy formed a certain amount of Ti_2Cu phase, which released Cu^{2+} through corrosion reaction in contact with the solution medium and had a strong antibacterial function [15]. However, Ti–Cu alloy is still a bioinert material to biological system.

Anodic oxidation (AO) can effectively adjust the surface morphology of titanium and titanium alloy and promote cell proliferation and adhesion. Studies have shown that a graded porous morphology on pure titanium improved the proliferation ability of osteoblasts and had good biological activity [16]. Botha [17] found that the anodic oxidation film had high bonding strength, good chemical stability, high decorative value and no toxic side effects on cells.

The experimental parameters in the anodic oxidation process significantly affect the characteristics of the oxide film and further affect the biocompatibility. Nano-modification, as one of the good options, had the potential to induce different degrees of antibacterial effect on the surface of implant materials [18]. Habazaki et al. [19] found that increasing the anodic oxidation voltage in alkaline electrolyte could reduce the porosity of the oxide film. Extending the oxidation time enhanced the crystallization of titanium oxide film [20–22], the thickness of the oxide coating [23] as well as the chemical composition. On the contrary, it was also reported that the time evolution of film thickness showed a downward trend, which may be due to dehydration of the oxide film on titanium [24]. So far, anodic oxidation has been commercially and widely used in the surface treatment of bone plates and screws.

Studies have shown that the main reason for the antibacterial ability of Ti–Cu was due to the antibacterial mechanism of Ti_2Cu contact [25]. However, the oxide coating on titanium alloys after anodic oxidation would separate Ti–Cu alloy from close contact with bacteria, which might reduce the antibacterial function of Ti_2Cu phases and the antibacterial properties. Therefore, the anodic oxidation was applied to Ti–Cu alloy in this study to reveal the anodic oxidation on the surface biocompatibility and antibacterial properties. The microstructure, corrosion resistance, antibacterial ability and cell compatibility were studied in detail. Primary research showed that the oxide coating significantly enhanced the corrosion resistance and the antibacterial properties and improved the cell adhesion and spreading. All these results show that the anodic oxidation could be used for Ti–Cu for biomedical application.

2 Experimental

2.1 Preparation of Ti–Cu sample

Commercially pure titanium (99.9%) and pure copper (99.9%) were used to prepare Ti–5 wt%Cu (Ti–5Cu, hereafter) alloys rods with a diameter of 15 mm in a consumable vacuum arc melting furnace followed by forging at 800–900 °C. Samples for the following experiment with thickness of 2 mm were cut from the alloy rod and sealed in a vacuum quartz tube, solution treated at 900–950 °C for 5 h and quenched, and then aged at 600 °C for 24 h to obtain the final Ti–5Cu samples.

2.2 Anodic oxidation (AO)

Ti–5Cu sample was polished with 80, 400, 800 and 1200 grit SiC sandpaper in sequence and then washed with 100% alcohol and dried. After this, the samples were surface activated in a mixture acid solution of $HF:HNO_3:H_2O$ = 1:2:50 (in volume ratio) for no more than 15 s, rinsed by tap water for about 30 s, ultrasonically cleaned in ethanol for 5 min and dried in air. Anodic oxidation (AO) was reacted in 0.1 mol·L^{-1} H_3PO_4 solution at a voltage value of 30 V for 1, 3, 5 and 10 min, hereinafter referred to as AO-1 min, AO-3 min, AO-5 min and AO-10 min samples in comparison with untreated sample (AO-0 min). Then, the samples were put into hot water for 30 min to seal the surface.

2.3 XRD and SEM/EDS

X-ray diffractometer (XRD, Smart Lab) was used to analyze the phase constitution at a scanning rate of 4 min^{-1} under following parameters: Cu target, Kα radiation with λ = 0.15405980 nm, tube voltage of 40 kV, tube current of 50 mA, and power of 18 kW. The phase composition was analyzed by X'Pert High Score software. Surface morphology and elemental composition analysis were conducted on a scanning electron microscope (SEM, JSM 6360LV, JEOL, Japan) equipped with energy-dispersive X-ray spectroscopy (EDS).

2.4 Surface roughness and water contact angle

The two-dimensional (2D) and three-dimensional (3D) surface roughness (R_a) was measured by a laser confocal microscope (OLS4100, OLYMPUS, Japan), and five areas

with a size of 100 μm × 100 μm were randomly selected. The contact angle of the sample surface was measured by a static contact angle meter (SL200KS, Kino Industry, USA). During the process, 1.5 μl ultrapure water was dropped on the surface and the water contact angle was measured by a software. In order to obtain an average with standard deviation, at least 3 points should be selected.

2.5 XPS

X-ray photoelectron spectrometer (XPS, JPS-9200) was used to analyze the valence and composition of the samples' oxide film. High-resolution scanning was performed on Ti, Cu and O. All spectral data were calibrated at a C 1s binding energy of 284.8 eV. XPS peak software was used to perform peak fitting processing on the original XPS data.

2.6 Corrosion resistance

VersaSTAT 300 electrochemical workstation was used to measure the electrochemical curves of different samples in a physiological saline (0.9% NaCl) solution. Power Suite and ZSimp Win were used to analyze and fit the spectra data. A three-electrode test system was adopted with the tested sample as the working electrode, saturated calomel electrode (SCE) as the reference electrode and platinum plate as the counter electrode for electrochemical experiments. Electrochemical impedance spectrum (EIS, VersaSTAT 300) was measured at a frequency from 0.01 to 1×10^5 Hz, and then Tafel curve was measured at a scanning rate of 0.5 mV·s^{-1}.

2.7 Ion release

Samples were immersed in physiological saline (0.9% NaCl) at 37 °C for 24 h with a ratio of surface area to solution volume of 1.25 cm^2·m^{-1}, and the Cu ion concentration in the solution was measured by inductively coupled plasma mass spectrometer (ICP-MS 2000).

2.8 Antibacterial properties

2.8.1 Plate count method

The antibacterial activity was evaluated according to GB/T 2591 (corresponding to JIS Z2801-2000 and ASTM G21-96) [26]. Staphylococcus aureus (*Saureus* ATCC 6538) was used as the test bacterium. Before the experiment, the experimental supplies were placed on a clean workbench for 1 h, and the nutrient broth (NB) and physiological agar were prepared according to the experimental standards. Appropriate amount (scrape 1–2 circles) of fresh bacterial solution to 37 °C liquid medium was used to prepare

100 μl bacterial solution, and 80 μl bacterial suspension with phosphate buffered saline (PBS, Gibco Oshima). The sample was placed in a 12-well plate, and 100 μl bacteria suspension was inoculated on the sample surface and distributed evenly to ensure that the bacteria suspension would not drip to the outside of the sample. Then, the plate containing the sample was placed in an incubator at (37 ± 1) °C and relative humidity (RH) ≥ 90% for 24 h. After the incubation, normal saline was added to each well to ensure that there were no bacteria on the sample; 100 μl solution was taken out of the well and was evenly dispersed with a triangular glass rod until there was no obvious liquid on the surface, and then incubated at (37 ± 1) °C and RH ≥ 90% for 24 h. According to Chinese National Standard (GB/T 4789.2–2010), the active bacteria were counted. The antibacterial rate (R) was calculated by the following formula:

$$R = (N_{\text{control}} - N_{\text{sample}})/N_{\text{control}} \times 100\% \qquad (1)$$

where N_{control} and N_{sample} are the colonies number on the control sample (cp-Ti) and the test sample, respectively. According to Chinese National Standard (GB/T 4789.2–2010), $R \geq 90\%$ indicates that the sample has antibacterial properties, and $R \geq 99\%$ indicates that the sample has strong antibacterial properties.

2.8.2 Dead/live staining

The live/dead BacLightTM kit (Thermo Fisher Scientific Inc, Waltham, MA, USA) was used to stain the bacteria. The kit is composed of SYTO-9 and propidium iodide (PI). The two agents were mixed with sterile distilled water at a ratio of 1:1, stored at − 20 °C and protected from light. 80 μl bacteria suspension was dropped on the sample in a dark environment and cultured for 24 h. After being stained for 10 min, the bacteria were observed under a fluorescent microscope. The green fluorescence was live bacteria, and the red fluorescence was dead bacteria.

2.9 Cell compatibility

2.9.1 MTT assay

MC3T3 cells were seeded at a density of 2×10^4 cells·ml^{-1} per well onto the samples separately placed in 24-well culture plates and allowed to grow for present time periods. Following cell growth, an methylthiazolyldiphenyl-tetrazolium bromide (MTT) solution prepared with PBS was added into each well and incubated for 4 h in the dark. Thereafter, 500 μl dimethyl sulfoxide (DMSO) was added in each well, and the plate was placed on a shaker for 10 min, then 100 μl mixed solution was transferred into 96-well plate, and the optical density (OD)

was measured using a microplate reader at 570 nm. The relative growth rate (RGR) was calculated as follows:

$$RGR = (OD_{sample} - OD_{control}) / (OD_{negative} - OD_{control}) \times 100\% \qquad (2)$$

where $OD_{negative}$, OD_{sample} and $OD_{control}$ are the optical density of the negative sample, the control sample and the test sample, respectively.

2.9.2 Cell morphology

MC3T3 cells were seeded onto samples surfaces as described in Sect. 2.9.1. After 1-, 4- and 24-h incubation, the samples were washed with PBS and fixed in 4% paraformaldehyde (PFA) solution for 20 min at 37 °C. 0.5% Triton X-100 was added to penetrate cell membrane for 5 min, and then the samples were washed with PBS. Phantom cyclic peptide was added and incubated for 30 min in a dark environment; then the cells were treated with DAPI (4,6-diamino-2-phenyl indole) for 2 min. Finally, the samples with cells were observed and recorded under a fluorescence microscope.

2.9.3 Statistic

All experiments were performed three times and expressed as mean ± standard deviation. Quantitative statistical analysis of representative results, $p < 0.05$ was considered statistically significant.

3 Results and discussion

3.1 Phase identification and microstructure

As shown in XRD patterns of Ti–5Cu samples treated with AO at different time (Fig. 1a), after being oxidized for 5 min, the oxide layer was mainly composed of α-Ti phases and Ti_2Cu phases, but no titanium and copper oxide was detected. At the same time, the peak intensity of Ti_2Cu phase decreased with the extension of the oxidation time, suggesting that the coating became thick with the extension of the oxidation. Figure 1b–e shows the appearance of AO-treated samples. After AO treatment, all samples were in blue color. The film color of Ti–Cu samples became dark blue gradually with the extension of the oxidation time.

3.2 Surface morphology and EDS

Figure 2a–d shows microscopic morphology of the AO-treated Ti–5Cu samples. When the oxidation time was 1 min, many scratches on the surface were seen clearly, as shown in Fig. 2a. White flower bud structures were also observed. When the oxidation extended to 3 min, flower-like structures with a small number of petal-like structures appeared on the surface, and the size of the flower-like structures increased at high magnification. When the oxidation time was 5 min, nearly all the surface was covered by the flower-like structure. After being oxidized for 10 min, as shown in Fig. 2d, the surface became smooth with few shallow scratches, indicating that a thick oxide coating was formed on the surface. Many flower-like structures with a size of 1 μm were seen on the surface. With the extension of the oxidation duration, the size of the flower-like structure increased.

Figure 2a1–d1 shows cross-sectional microstructures of the AO-treated Ti–5Cu samples. It can be seen that a double-layer coating with a thickness of 3–7 μm with a dense inside and porous outside was formed after anodization. With the extension of the oxidation time, Cu content in the coating gradually increased, and the dense layer had more Ti and Cu, as listed in Table 1. At the oxidation time of 1 min, the coating consisted of a dense layer with 1.7 μm in thickness and a porous layer with about 5.0 μm in thickness, as listed in Table 2. After 3-min oxidation, the coating thickness decreased slightly, but the dense layer grew rapidly to about 2.9 μm in thickness while the porous layer became denser. After 5-min oxidation, the thicknesses of the whole coating, the porous layer and the dense layer were all continuously reduced. After 10 min, the thickness of the film was reduced to about 3 μm, but the dense layer was stabilized at about 2.0 μm. In comparison with the cross-structure of the coating at 1 min, the coating became much denser and the surface became smoother with the extension of the oxidation time.

3.3 XPS

As examples, Fig. 3 shows XPS spectra of AO-3 min and AO-10 min samples. The diffraction peaks of Ti, O and Cu were detected in all samples. In the spectra of Cu (Fig. 3a, a1), Cu $2p_{3/2}$ peak at 932.92 eV and Cu $2p_{1/2}$ peaks at 952.64 and 945.71 eV were detected, which confirms the existence of Cu_2O and CuO in the oxidation coating [26, 27]. From the diffraction intensity, it can be deduced that Cu mainly existed as Cu_2O with a few CuO. Extension of the oxidation time did not bring about significant difference in Cu spectra, suggesting that the existing form of Cu and the relative content did not change with oxidation time. In Ti spectra of AO-3 min sample (Fig. 3b), Ti 2p spectrum can be decomposed into 5 small peaks, Ti $2p_{1/2}$ at 464.71 eV and Ti $2p_{3/2}$ at 458.85 eV, corresponding to TiO_2 [28, 29]; Ti $2p_{1/2}$ peak at 460.71 eV and Ti $2p_{3/2}$ peak
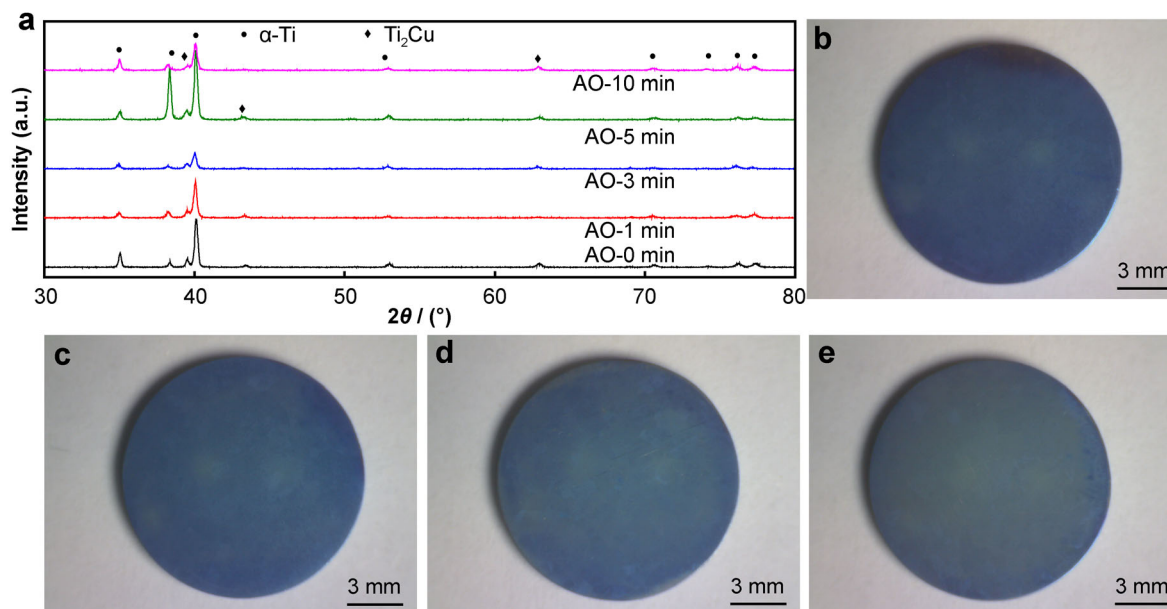
Fig. 1 a XRD patterns of Ti–5Cu samples treated with AO at different time; **b** AO-1 min, **c** AO-3 min, **d** AO-5 min, **e** AO-10 min surface appearance of Ti–5Cu alloy samples

at 457.28 eV, belonging to Ti_2O_3; Ti $2p_{1/2}$ peak at 463.14 eV, belonging to oxide colloid [30]. From the intensity, Ti mainly existed in TiO_2 with small amount of Ti_2O_3 oxide colloid. After 10-min oxidation, there was nearly no difference in the existing form of Ti in comparison with AO-3 min sample, as shown in Fig. 3b1. In O 1s spectra in Fig. 3c, O 1s spectrum was consisted of three diffraction peaks at 530.2, 530.76 and 531.19 eV, corresponding to Ti–O, Cu–O and C–O, respectively [23, 31]. With the extension of the oxidation time to 10 min, no new peak was detected. With the consideration of Cu and Ti spectra, O mainly existed in form of TiO_2, Cu_2O or CuO.

3.4 Wettability, roughness and ion release

Figure 4a shows the result of the roughness of Ti–5Cu samples with oxidation duration. When the oxidation time was 1 min, the roughness was larger than that of the untreated sample. With the extension of the oxidation to 5 min, there was nearly no change in the roughness. However, after 10-min oxidation, the surface roughness increased sharply to about 4–6 μm. Figure 4b shows the water contact angle of Ti–Cu samples before and after oxidation. Compared with the untreated Ti–5Cu sample, the contact angle of AO-treated Ti–5Cu samples decreased with the extension of the oxidation time, indicating that the hydrophilicity became better. Figure 4c shows the dissolved Cu ion concentration after immersing the Ti–5Cu sample in physiological saline for 24 h. It can be found that the Cu ion concentration increased obviously as the anodic

oxidation reached the highest value at 5 min and further oxidation reduced the Cu ion release significantly.

3.5 Electrochemical testing

The electrochemical correlation analysis of Ti–Cu samples in normal saline before and after anodization is shown in Fig. 5. It can be found from open current potential (OCP) curves in Fig. 5a and the self-corrosion open current potential (E_{ocp}) value in Table 3 that the corrosion potential of the samples after AO treatment was significantly higher than that of Ti–5Cu-based alloy, showing that AO treatment can significantly alleviate the corrosion tendency of Ti–5Cu alloy. Also, the longer the oxidation time was, the higher the corrosion potential was. The Tafel curve in Fig. 5b shows that AO treatment moved the curve toward more positive potential and high current density direction. The self-corrosion potential (E_{corr}) and the self-corrosion current density (i_{corr}) extrapolated from the Tafel curve are listed in Table 3. The self-corrosion current density decreased from 1.85×10^{-7} A·cm^{-2} for the untreated Ti–5Cu sample to 1.08×10^{-7}, 0.89×10^{-7}, 0.54×10^{-7}, 0.66×10^{-7} A·cm^{-2} with the increase in AO treatment duration, indicating that AO treatment reduced the corrosion current density or improved the corrosion resistance. In Fig. 5c, the capacitive arc radius after AO treatment was significantly larger than that of the untreated Ti–Cu sample, showing that AO coating had a good resistance to the corrosion solution. Figure 5d, e shows Bode curve at different oxidation time. The impedance value of the anodized
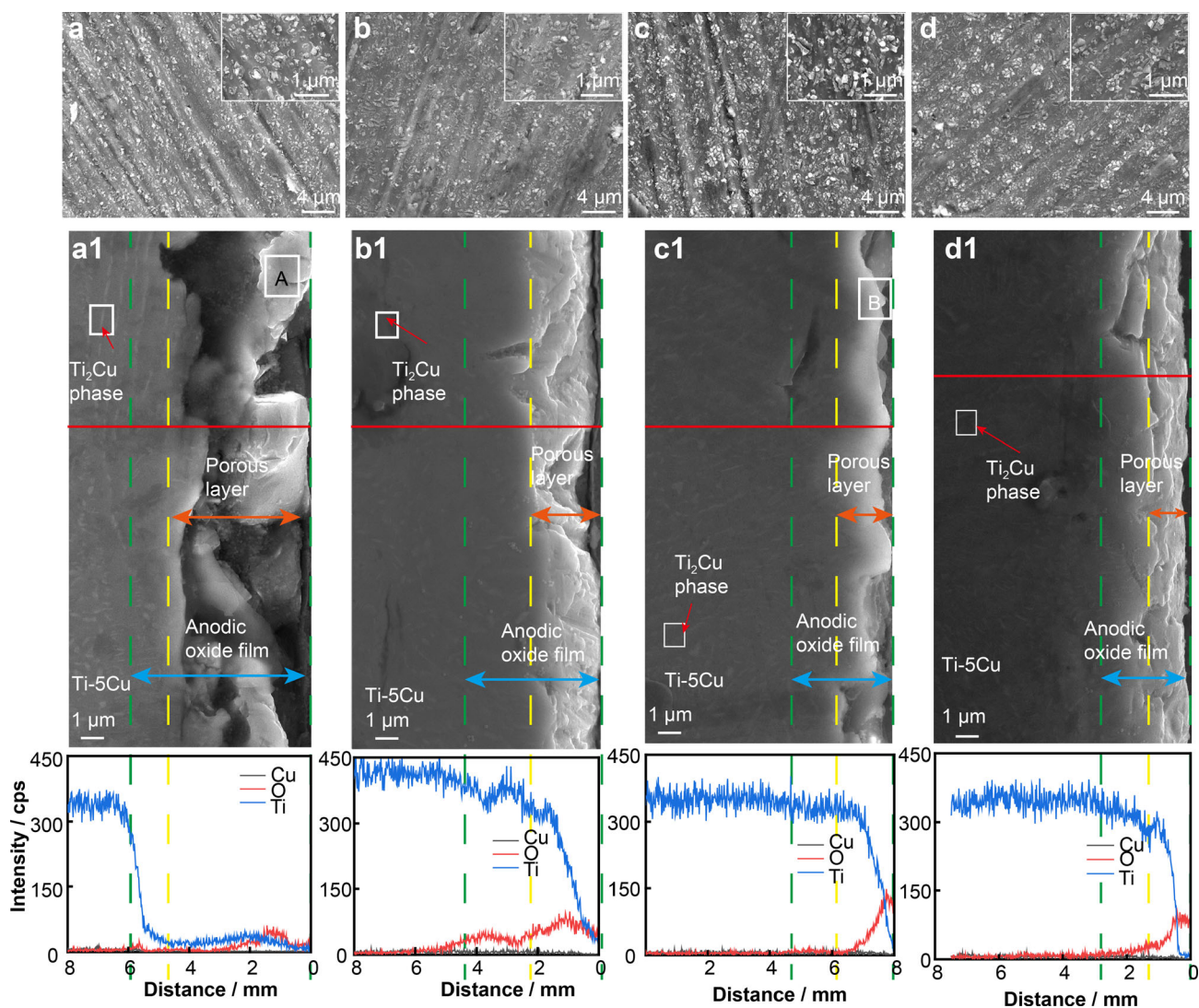
Fig. 2 Surface and cross-sectional microstructure morphology of AO treated Ti–5Cu samples; **a, a1** AO-1 min; **b, b1** AO-3 min; **c, c1** AO-5 min; **d, d1** AO-10 min

sample was higher. As shown in Fig. 5f, g, the equivalent circuit model was used to simulate the structure of the passivation film. The calculated electrochemical data are shown in Table 4. The corrosion resistance of Ti–Cu sample was improved by AO treatment and increased with the extension of AO treatment, indicating that the anodic oxide coating, as an insulator with a thickness of about 4–6 μm, had large corrosion resistance and could protect Ti–5Cu base alloy from solution attacking.

3.6 Antibacterial properties

3.6.1 Antibacterial rate

Figure 6a–f shows typical bacteria colonies after 24-h incubation on Ti–Cu samples. On cp-Ti, many bacteria

colonies were found, as shown in Fig. 6a, confirming that cp-Ti does not have antibacterial effect. There were only a few colonies on Ti–Cu sample and no colony on the AO-treated Ti–5Cu samples, indicating that *S. aureus* were all dead after 24-h incubation on Ti–Cu samples. The antibacterial rates curve in Fig. 6g demonstrated that the antibacterial rate of Ti–Cu sample and AO-treated Ti–Cu sample was > 99%.

3.6.2 Live/dead staining

Figure 7 shows live/dead staining of *S. aureus* co-cultured on Ti–5Cu samples for 24 h. The fluorescent green on the surface of cp-Ti was significantly more than red, showing that *S. aureus* adhered and proliferated well on cp-Ti. On the surface of AO-treated samples, only red fluorescence

Table 1 EDS results of cross-sectional microstructure of AO treated Ti–5Cu samples

Oxidation time	Position	Element	w/wt%	x/at%
1 min	Porous layer	Ti	59.86	33.35
		Cu	1.86	0.78
	Dense layer	Ti	67.77	41.21
		Cu	5.30	2.43
5 min	Porous layer	Ti	69.85	47.34
		Cu	5.65	2.88
	Dense layer	Ti	70.99	45.32
		Cu	6.47	3.11
3 min	Porous layer	Ti	43.63	20.83
		Cu	4.81	1.73
	Dense layer	Ti	61.28	35.32
		Cu	5.21	2.26
10 min	Porous layer	Ti	71.78	47.54
		Cu	5.00	2.49
	Dense layer	Ti	76.27	55.58
		Cu	7.04	3.87

Table 2 Thickness of oxide coating on AO treated Ti–5Cu samples (μm)

Samples	AO-1 min	AO-3 min	AO-5 min	AO-10 min
Thickness of Anodic oxide coating	6.7 ± 0.2	5.5 ± 0.1	4.0 ± 0.1	3.0 ± 0.05
Thickness of porous layer	5.0 ± 0.2	2.6 ± 0.05	2.0 ± 0.1	1.0 ± 0.2
Thickness of dense layer	1.7 ± 0.1	2.9 ± 0.1	2.0 ± 0.1	2.0 ± 0.05

was observed, indicating that *S. aureus* could not survive on the AO-treated samples and all bacteria were killed; these results were consistent with the results of the plate experiment.

3.7 Cell toxicity

Figure 8a shows optical density of MC3T3-E1 cells measured by MTT after 1-, 3-, and 5-day incubation on cp-Ti and Ti–Cu samples. The results showed that with the extension of culture time, the number of cells on the samples surface increased. On the first day, no difference was found between OD values of cp-Ti and Ti–Cu samples and among the values of Ti–5Cu samples. On the third day, OD value of Ti–Cu sample was lower significantly than

that of cp-Ti, and OD values of AO-treated Ti–Cu samples were obviously lower than that of Ti–Cu sample, but no difference was observed among OD values of AO-treated Ti–Cu samples. However, on the fifth day, OD values of Ti–Cu samples were obviously higher than that of cp-Ti and no difference was found among the OD values of Ti–Cu samples. Figure 8b shows the calculated RGR of cells. RGRs of Ti–Cu samples were less than 100% but higher than 75% on the first day and the third day, corresponding to cell cytotoxicity of Grade 1. However, RGRs of Ti–Cu samples were higher than 100% on the fifth day, corresponding to Grade 0. All these results demonstrated that Ti–Cu samples including the AO-treated samples did have no cytotoxicity to MC3T3-E1 cells.

Figure 9 shows cell adhesion and spreading activities of MC3T3-E1 cells co-cultured on the samples for up to 24 h. After 1-h culture, the cells showed spherical shape on the samples. With the extension of oxidation time, more actin filaments were expressed on the surface and the spreading area increased. After 24-h culture, the cells on the AO-treated Ti–Cu samples showed stronger actin, filamentous pseudopodia and lamellar pseudopodia signals compared with that on cp-Ti. These results show that the anodized samples could improve the adhesion and spreading effect of MC3T3-E1 cells. However, the Ti–Cu samples with different oxidation time showed no difference in cell morphology.

4 Discussion

4.1 Formation of anodic oxidation coating and surface physical properties

The AO coating on titanium alloy was formed by electrolytic extraction of O^{2-} and metal element in the base alloy. Surface appearance in Fig. 1b–e clearly showed that an oxide coating was formed on the surface with blue color. SEM results indicated that an oxide coating with a dense inside and a porous outside was formed on Ti–Cu sample after anodic oxidation. The coating became denser and denser with the oxidation time prolonging, as shown in Fig. 2a1–d1. A "flower-like" structure had shown a connected growth form on the oxide coating when the oxidation time was about 10 min. It was reported that this structure was actually the performance of the dielectric breakdown of the coating [32–34]. Figures 1a, 3 show that the oxide film was mainly composed of TiO_2, Cu_2O and small amount of CuO, and the extension of the oxidation time had limited effect on the chemical composition and phase constitution.

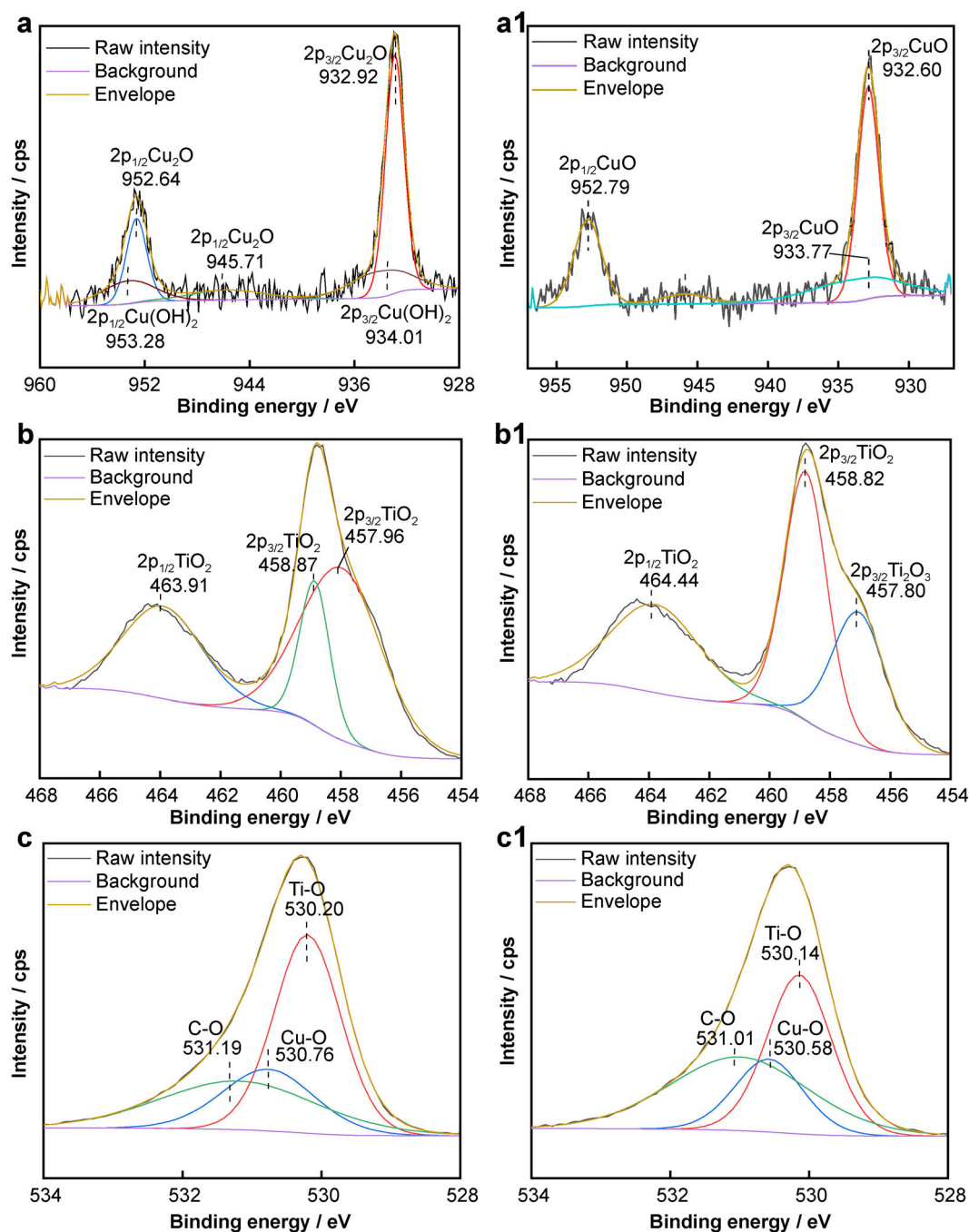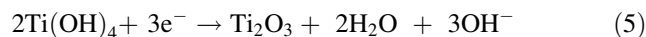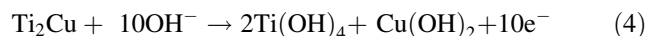At the initial stage of the anodization process of Ti–5Cu, a violent hydrolysis reaction occurred first in the

Fig. 3 XPS analysis spectra of AO-3 min and AO-10 min samples: **a** Cu 2p, **b** Ti 2p and **c** O1s spectra of AO-3 min sample; **a1** Cu 2p, **b1** Ti 2p and **c1** O 1s spectra of AO-10 min sample

electrolyte, producing a large amount of free OH^- according to following reaction:

$$2H_2O \ + \ 2e^- \rightarrow H_2 \uparrow + 2OH^- \qquad (3)$$

Then, the free OH^- first reacted with α-Ti in the preferential dissolving of Ti from the Ti–Cu alloy. As the surrounding matrix dissolved, Ti_2Cu particles were gradually exposed, separated from the matrix and

released into the solution. Then, the following two reactions happened on the surface:

$$Ti_2Cu + \ 10OH^- \rightarrow 2Ti(OH)_4 + Cu(OH)_2 + 10e^- \qquad (4)$$

$$2Ti(OH)_4 + 3e^- \rightarrow Ti_2O_3 \ + \ 2H_2O \ + \ 3OH^- \qquad (5)$$

Subsequently, Reactions (6–8) occurred on the surface, a large amount of Cu^{2+} migrated outwards, and the dense
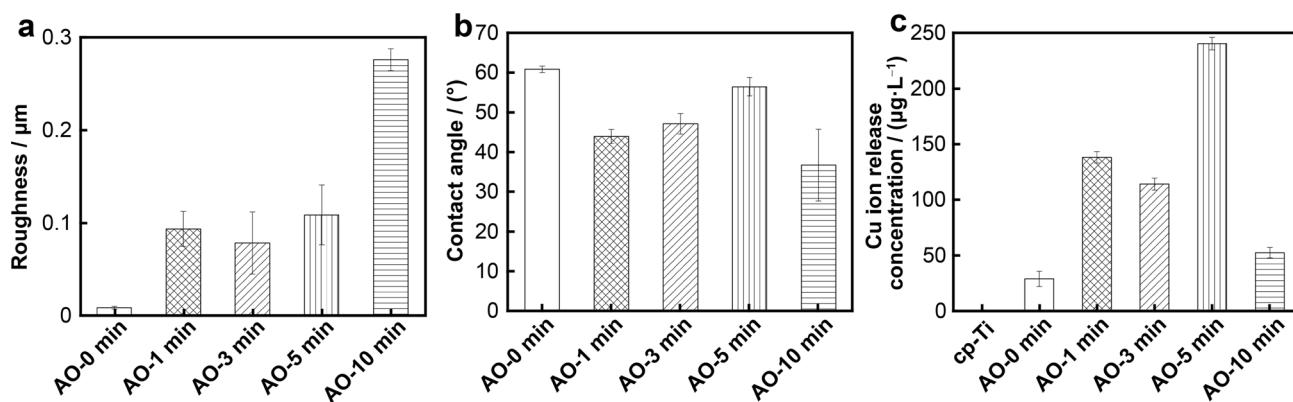
Fig. 4 **a** Roughness, **b** water contact angle and **c** Cu ion release concentration from different samples after 24-h immersion in 0.9%NaCl
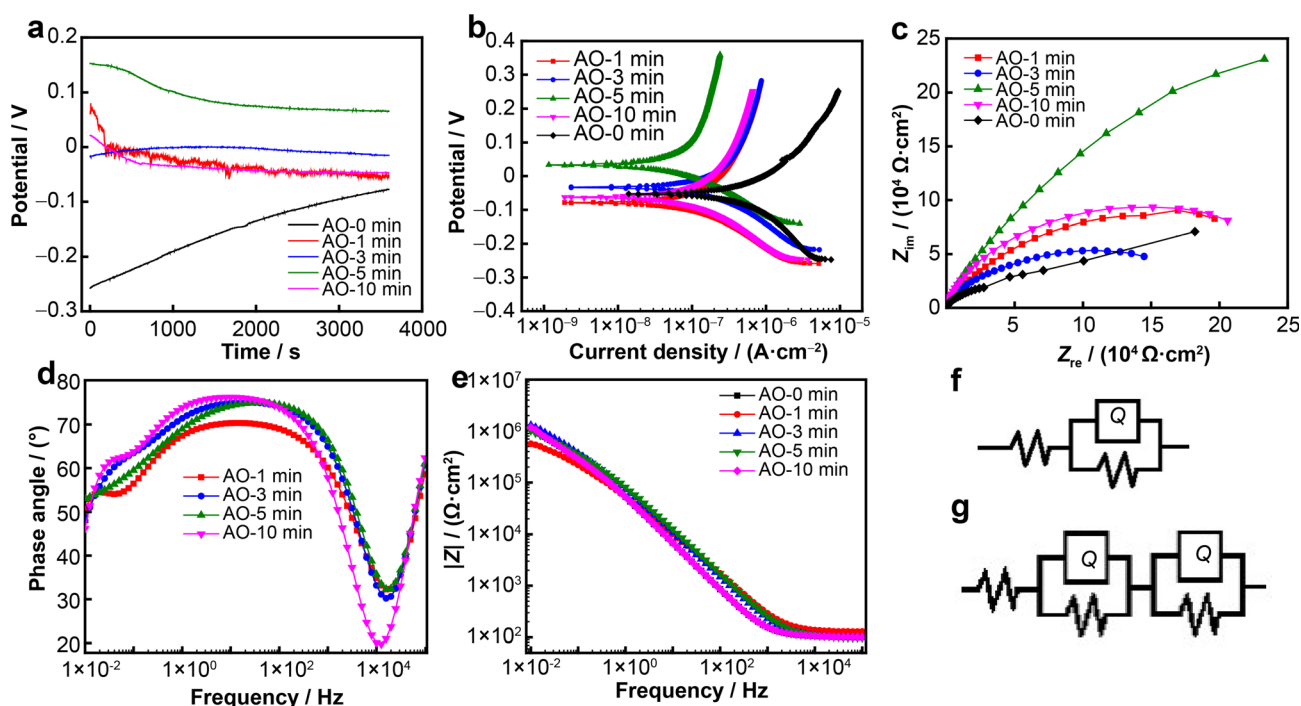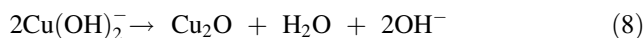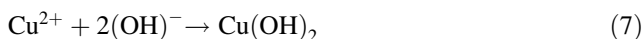

Fig. 5 Electrochemical curves of Ti–5Cu samples: **a** Open-circuit potential (OCP); **b** Tafel curves; **c** Nyquist curves; **d, e** Bode and Bode phase curves; **f** equivalent circuit model of AO-0 min sample; **g** equivalent circuit model of others samples

film on the surface was destroyed by continuous electrolysis, as shown in Fig. 10a. Cu^{2+} began to react with the appearance of pores outside the dense layer. When adjacent pores converged, larger pores would be formed. The outer porous layer changed from a granular structure to a lamellar structure, resulting in the appearance of a "flowering" structure, as shown in Fig. 10b.

$$2Ti_2O_3 + O_2 \rightarrow 4TiO_2 \tag{6}$$

$$Cu^{2+} + 2(OH)^- \rightarrow Cu(OH)_2 \tag{7}$$

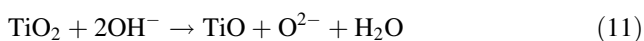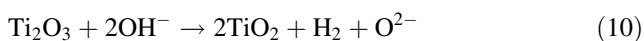$$2Cu(OH)_2^- \rightarrow Cu_2O + H_2O + 2OH^- \tag{8}$$

As the oxidation progressed, a film layer would be formed continuously on the outside. With the generation of oxygen, the barrier layer was thick enough that O^{2-} could not penetrate under the electric field applied by the current voltage. At this time, the formation rate of the oxide film and the dissolution rate reached a balance. The film thickness did not change, and the flowering structure grew to the best state with time. As the oxidation time prolonged,

Table 3 Self-corrosion potential and self-corrosion current density of different samples

Samples	E_{ocp}/V (vs. SCE)	E_{corr}/V (vs. SCE)	i_{corr}/ (10^{-7}A·cm^{-2})
AO-0 min	-302.72 ± 14.37	-0.148 ± 0.019	1.85 ± 0.21
AO-1 min	-53.95 ± 32.52	-0.078 ± 0.012	1.08 ± 0.09
AO-3 min	49.69 ± 23.42	-0.033 ± 0.013	0.89 ± 0.08
AO-5 min	59.59 ± 15.45	0.031 ± 0.01	0.54 ± 0.07
AO-10 min	-109.8 ± 11.26	-0.062 ± 0.014	0.66 ± 0.04

the flowers were connected together, as shown in Fig. 10c. The dense and porous layers began to hydrolyze according to Reactions (9–11) and release a small amount of Cu^{2+}. As a result, CuO and TiO$_2$ were produced oxides on the coating surface.

$$Cu^{2+} + O^{2-} \rightarrow CuO \tag{9}$$

$$Ti_2O_3 + 2OH^- \rightarrow 2TiO_2 + H_2 + O^{2-} \tag{10}$$

$$TiO_2 + 2OH^- \rightarrow TiO + O^{2-} + H_2O \tag{11}$$

The greater the surface roughness of the titanium alloy is, the higher the specific surface area is, and the better the cell proliferation and adhesion effect is, which is conducive to the stable proliferation of cells on the surface [35]. As shown in Fig. 4a, the roughness of Ti–Cu sample continued to increase with the extension of anodization time, indicating that the flowering structure formed by electron migration and bonding had a significant impact on cell proliferation and adhesion significantly. When the surface contact angle was less than 60°, the greater the roughness was, and the better the hydrophilicity was [31]. When the surface contact angle was above 60°, the greater the roughness was, the better the hydrophobicity was. As shown in Fig. 4b, the flowering structure (< 60°) improved hydrophilicity.

4.2 Corrosion resistance and ion release

Previous studies on Ti–Cu alloys have indicated that the second phase of Ti$_2$Cu in Ti–Cu alloys slightly improved the anti-corrosion properties [36]. The electrochemical results in Fig. 5 clearly demonstrated that the AO coating improved the open corrosion potential and reduced the corrosion current density. Also, a high phase angle and large corrosion resistance were found on the AO-treated samples, indicating that the coating provided reasonable protection for Ti–5Cu substrate and effectively improved the corrosion resistance. As mentioned before, a double-layer coating was formed on the surface of Ti–Cu alloy. The dense inner oxide layer could provide good protection against solution attacking, as indicated by the high phase angle and high corrosion resistance in Fig. 5d, e. da Fonseca et al. [22] found that the film structure existing in the titanium oxide film was amorphous. Habazaki et al. [37] reported that when the titanium alloy was first anodized, subnano-sized oxides were produced on the surface, and the grain size of these oxides gradually increased over time.

With the extension of oxidation time up to 5 min, the corrosion current density decreased and the corrosion resistance increased significantly, as listed in Tables 3, 4. However, further extension of oxidation time did not improve the anti-corrosion properties. Microstructure observation in Fig. 2a1–d1 indicated that the coating became denser with the extension of the oxidation time in the first 5 min, which provided good protection, and the further extension of the oxidation time to 10 min resulted in limited improvement in the coating structure. EIS results in Fig. 5 also confirmed that there was no significant difference in the phase angle and the corrosion resistance between AO-5 min and AO-10 min samples.

Although the oxide coating could reduce the corrosion current density significantly, a higher Cu ion was released from AO-treated sample than Ti–Cu-based alloy, as reported in Fig. 4c. At the beginning of the oxidation, the coating was mainly porous and the dense layer was very thin; at this time, the content of Ti and Cu in the coating was low, as shown in Fig. 2a1–d1. Therefore, more Cu ions were released from the porous coating as well as from Ti–Cu-based alloy. However, after 10-min oxidation, the AO coating became much dense, which inhibited the

Table 4 EIS curve data of Ti–5Cu alloy after AO treatment for different oxidation time

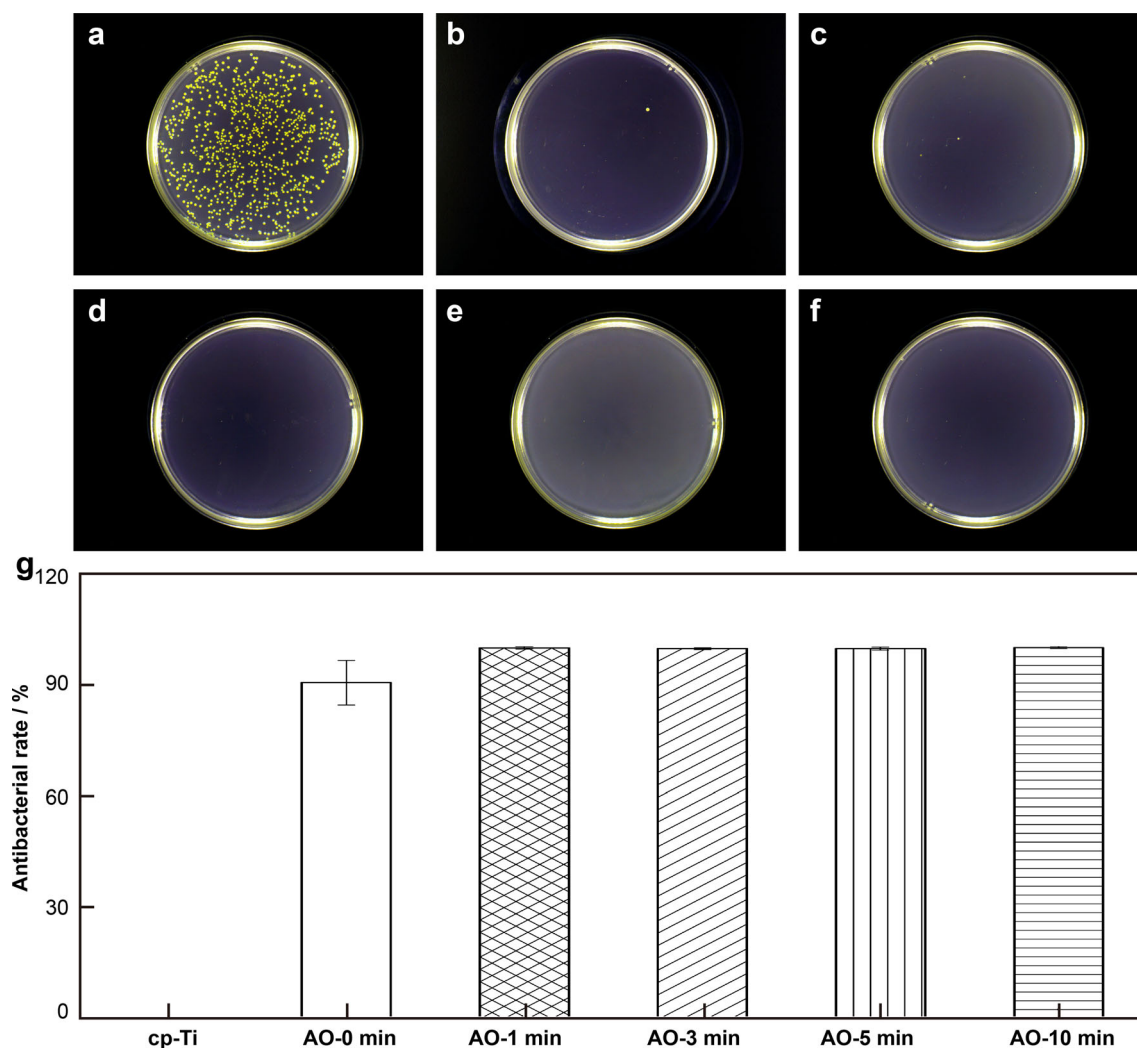| Samples	R_s/(Ω·cm^2)	Q_p/(10^{-5} S·cm^2·s^{-n})	R_p/(10^4 Ω·cm^2)	n_p	R_{Cp}/(10^5 Ω·cm^2)	Q_{ds}/(10^{-5} S·cm^{-2}·s^{-n})	n_b
AO-0 min	72.36 ± 0.18	2.53 ± 0.02	7.33 ± 0.39	0.93 ± 0.00	–	–	–
AO-1 min	89.98 ± 0.48	0.27 ± 0.15	5.38 ± 1.21	0.88 ± 0.01	6.13 ± 0.13	0.51 ± 0.13	0.57 ± 0.01
AO-3 min	68.89 ± 0.41	0.34 ± 0.05	16.55 ± 0.27	0.87 ± 0.00	19.19 ± 0.23	0.29 ± 0.20	0.55 ± 0.04
AO-5 min	69.91 ± 0.59	0.28 ± 0.09	7.60 ± 4.28	0.88 ± 0.00	52.08 ± 56.83	0.37 ± 0.33	0.37 ± 0.06
AO-10 min	72.38 ± 0.51	0.48 ± 0.00	24.53 ± 0.27	0.90 ± 0.00	54.00 ± 2.95	0.56 ± 0.52	0.65 ± 0.05

Fig. 6 Typical bacterial colonies on different samples: **a** cp-Ti; **b** AO-0 min (Ti–5Cu); **c** AO-1 min; **d** AO-3 min; **e** AO-5 min; **f** AO-10 min; **g** antibacterial rate

dissolution of Cu^{2+}. So, the Cu ion release was significantly reduced from AO-10 min sample.

4.3 Antibacterial Properties

Ti–Cu alloy exhibited strong antibacterial properties against *S. aureus* [15]. As mentioned earlier, the Ti_2Cu phase in Ti–Cu alloy had antibacterial properties [38–40]. The anodic oxide coating on Ti–5Cu sample separated Ti_2Cu phase from close contact with bacteria and improved the hydrophilicity, and in turn would accelerate the cell adhesion including bacteria and reduce the antibacterial ability as a result. However, the AO-treated Ti–5Cu samples exhibited high antibacterial rate of ≥ 99.99%, as shown in Figs. 6, 7, indicating that the AO coating inhibited the growth of bacteria. Microstructure analysis in above section indicated that the oxide coating on AO samples mainly consisted of TiO_2, Cu_2O and a small amount of CuO. It has been reported that TiO_2 exhibited antibacterial ability under UV light [41]. In this study, the bacteria were incubated on samples in a dark condition. Therefore, the antibacterial properties of TiO_2 were not activated in this study.

Many reports have shown that CuO nanoparticles were effective against methicillin-resistant Staphylococcus aureus (MRSA), *E. coli*, Pseudomonas aeruginosa, Klebsiella pneumoniae, Enterococcus faecalis, Shigella flexneri, mice Salmonella typhi, Proteus vulgaris, *S. aureus* and fungal strains Aspergillus niger and Candida albicans [29, 42–44]. It was also reported that Cu_2O in the surface coating of titanium had great antibacterial effect against MRSA [45–48]. He et al. [49] found that drug-loaded multilayers could inhibit the growth of bacteria on Ti substrate. Therefore, it can be easily deduced that CuO and Cu_2O in the oxide coating could inhibit the proliferation of the bacteria and achieve the antibacterial effects.
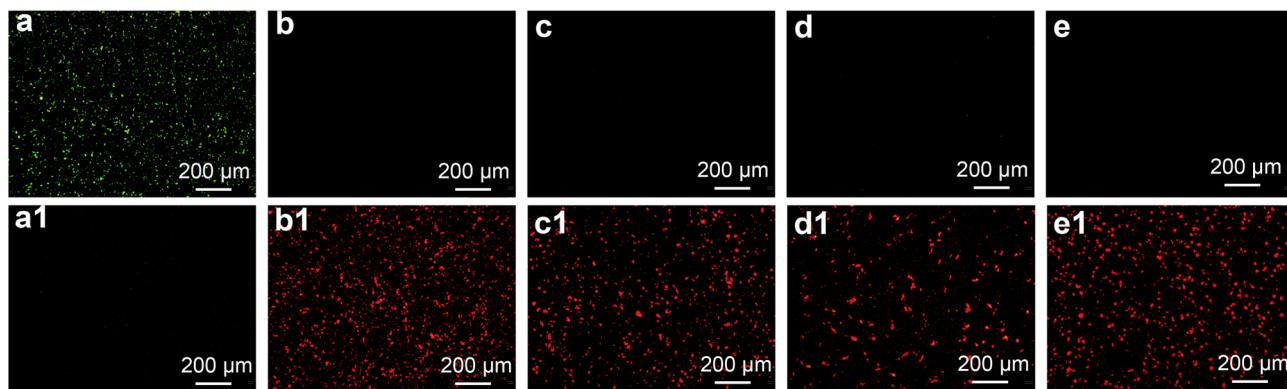
Fig. 7 Live and dead staining of bacteria on Ti–5Cu samples: **a, a1** cp-Ti; **b, b1** AO-1 min; **c, c1** AO-3 min; **d, d1** AO-5 min; **e, e1** AO-10 min
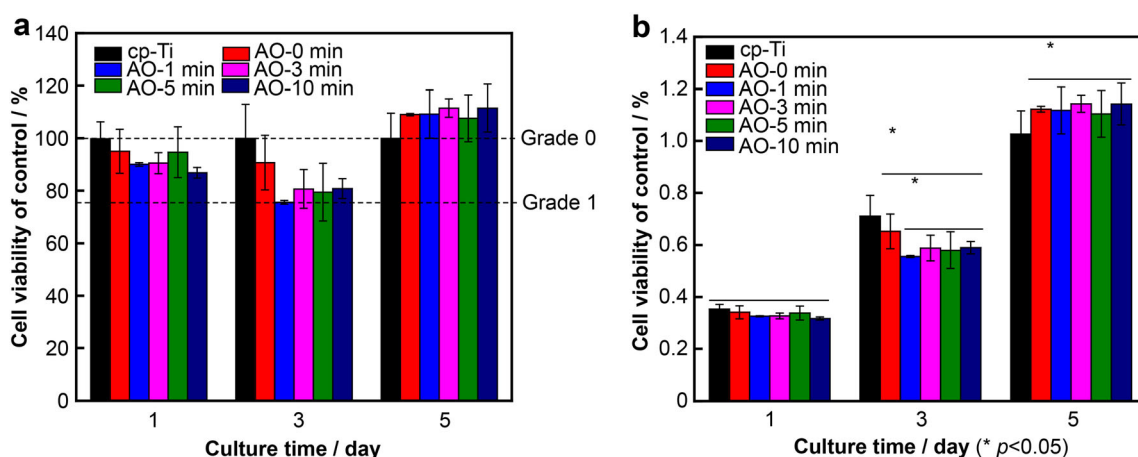

Fig. 8 Viability of MC3T3 cells direct contact with different samples for 1 day, 3 days and 5 days (*$p < 0.05$): **a** OD value; **b** cell viability

High Cu ion release was detected after AO treatment, as shown in Fig. 4c. When the sample was incubated with bacteria suspension, Cu ion would be released from the coating as discussed in the above section. Cu ion concentration would be as high as 50–250 μg·L^{-1}. Although Cu ion release concentration from AO-treated sample was less than recommended minimum ion concentration (MIC) value of Cu ion against *S. aureus* (300 μmol·L^{-1}) [50], Cu ions could still bind closely to the surface of negatively charged bacteria through Coulomb interactions, resulting in an imbalance of the inner and outer membrane potential [10], thus causing oxidative stress, producing reactive oxygen species (ROS), inducing cell wall damage and protein damage and ultimately leading to the death of bacteria [51]. In summary, the antibacterial properties of the AO-treated Ti–Cu sample were mainly attributed to the mixed function of the presence of Cu$_2$O and CuO, and Cu ion release.

4.4 Cell toxicity

Good cytocompatibility is a basic requirement for a biomedical material and surface modification for clinical application. The results of CCK-8 in Fig. 8 show that the cell viability of AO-treated Ti–Cu samples was higher than 75% at all intervals, indicating that no cell toxicity was found in comparison with cp-Ti sample. However, significantly low cell viability was observed on the anodic oxidized Ti–Cu samples in comparison with Ti–Cu matrix at the third day while significantly high cell viability was observed at the fifth day.

As mentioned in above section, the water contact angle of Ti–Cu sample was reduced after the anodic oxidation due to the petal-like and small flower-like structures, as shown in Fig. 2a–d. The smaller the water contact angle was, the better the hydrophilicity was, and the greater the surface energy was, which is more conducive to the
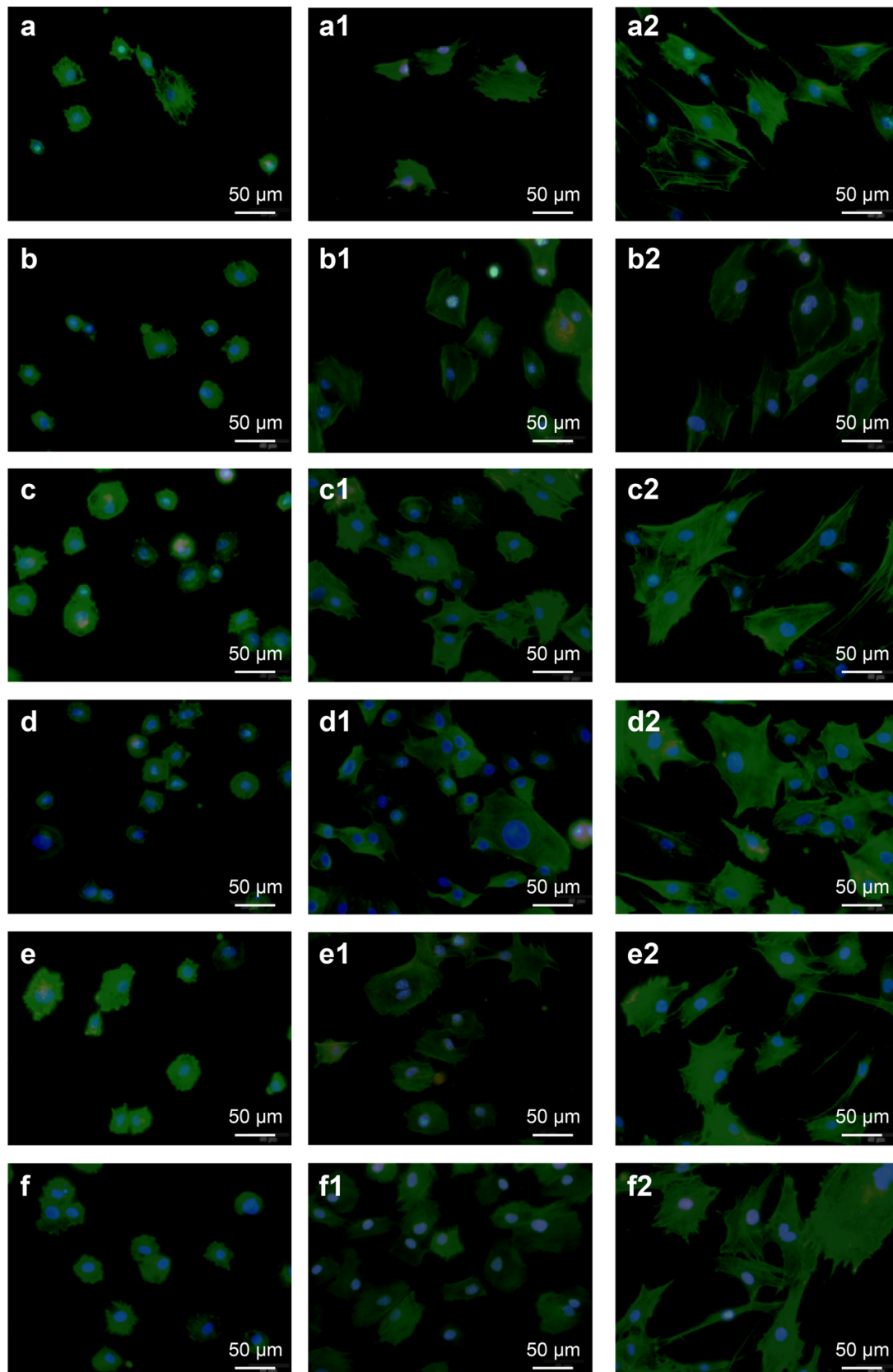
Fig. 9 Cytoskeletal actin and nuclear staining of MC3T3 cell on different samples after culturing for different time: **a**, **a1**, **a2** cp-Ti; **b**, **b1, b2** AO-0 min; **c, c1, c2** AO-1 min; **d, d1, d2** AO-3 min; **e, e1, e2** AO-5 min; **f, f1, f2** AO-10 min
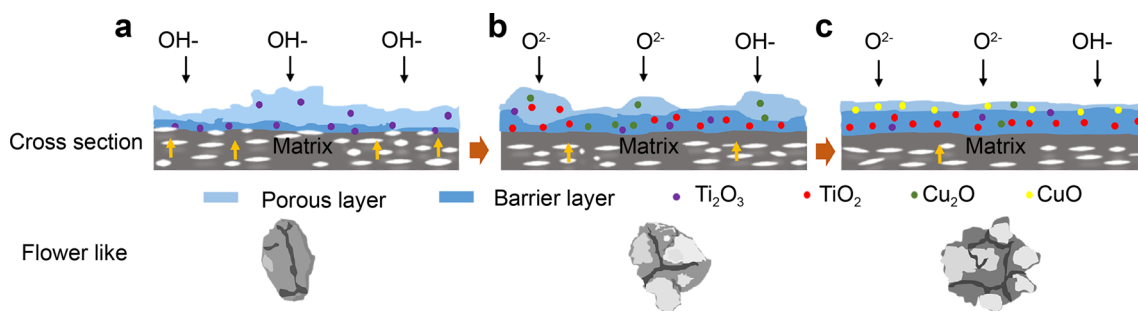
Fig. 10 Schematic diagram of Ti–5Cu anodizing process: **a** AO-3 min; **b** AO-5 min; **c** AO-10 min

adsorption and initial adhesion of proteins and cells [52, 53]. As a result, the adhesion and spreading ability of cells were enhanced on the AO-treated sample in comparison with cp-Ti and Ti–Cu samples, as shown in Fig. 9.

At the same time, titanium oxide was formed on Ti–5Cu sample after oxidation. Studies have shown that both anatase and rutile had good biological activity and osteoinductive properties [30, 54]. Therefore, TiO_2 or Ti_2O_3 on the surface could be conducive to cell adhesion and proliferation. After the anodic oxidation, more Cu ion was released in comparison with Ti–Cu base alloy, as shown in Fig. 4c. Cu ion release concentration from the AO-treated Ti–Cu sample in 24 h was in a range of 52–239 $\mu g \cdot L^{-1}$. Copper is helpful in the formation of blood vessels and in the formation of new bone. An appropriate amount of copper ions can promote the release of growth factors from human cells, which is conducive to the differentiation of osteoblasts and the deposition of calcium salts [55]. It has been confirmed that copper could stimulate the proliferation and differentiation of endothelial cells by increasing the direct or indirect expression of VEGF and HIF-1α in mesenchymal stem cells [56, 57]. The high Cu ion release might contribute to the high cell viability at the fifth day. However, high Cu ion concentration may also cause cell toxicity [58].

In summary, Ti–5Cu alloy modified by anodic oxidation exhibited better corrosion resistance and antibacterial effect than Ti–5Cu base alloy. The petal-like and small flower-like structures morphology on the surface was beneficial to the cell adhesion and proliferation. In addition, Cu ion release promoted the cell proliferation. However, further research is still necessary to reveal the in vivo antibacterial properties and cell compatibility in future.

5 Conclusion

A double-layer oxide coating with dense inner layer and porous outside layer was formed on Ti–Cu alloy. The oxide coating mainly consisted of Ti_2O, Cu_2O and small amount of CuO. The coating improved the corrosion resistance of Ti–Cu alloy by one order of magnitude and improved the antibacterial properties mainly due to the comprehensive function of CuO and Cu_2O. The porous outside layer enhanced the adhesion of MC3T3 cell and the release of Cu ion promoted the cell proliferation.

Declarations

Conflicts of interests The authors declare that they have no conflict of interests.

References

[1] Liu R, Memarzadeh K, Chang B, Zhang Y, Ma M, Allaker RP, Ren L, Yang K. Antibacterial effect of copper-bearing titanium alloy (Ti–Cu) against *Streptococcus mutans* and *Porphyromonas gingivalis*. Sci Rep. 2016;6:29985.

[2] Li BQ, Li CL, Wang ZX, Lu X. Preparation of Ti–Nb–Ta–Zr alloys for load-bearing biomedical applications. Rare Met. 2019; 38(6):571.

[3] Zhang ZZ, Zheng GT, Li HX, Yang L, Wang XY, Qin GW, Zhang EL. Anti-bacterium influenced corrosion effect of antibacterial Ti-3Cu alloy in *Staphylococcus aureus* suspension for biomedical application. Mater Sci Eng C Mater Biol Appl. 2019;94:376.

[4] Liu J, Li FB, Liu C, Wang HY, Ren BR, Yang K, Zhang EL. Effect of Cu content on the antibacterial activity of titanium-copper sintered alloys. Mater Sci Eng C Mater Biol Appl. 2014;35:392.

[5] Ma Z, Li M, Liu R, Ren L, Zhang Y, Pan H, Zhao Y, Yang K. In vitro study on an antibacterial Ti–5Cu alloy for medical application. J Mater Sci Mater Med. 2016;27(5):91.

[6] Wang XY, Dong H, Liu J, Qin GW, Chen DF, Zhang EL. In vivo antibacterial property of Ti–Cu sintered alloy implant. Mater Sci Eng C. 2019;100:38.

[7] Cai DG, Zhao XT, Yang L, Wang RX, Qin GW, Chen DF, Zhang EL. A novel biomedical titanium alloy with high antibacterial property and low elastic modulus. J Mater Sci Technol. 2021;81:13.

[8] Zhang EL, Zhao XT, Hu JL, Wang RX, Fu S, Qin GW. Antibacterial metals and alloys for potential biomedical implants. Bioact Mater. 2021;6(8):2569.

[9] D'Addona A, Ghassemian M, Raffaelli L, Manicone PF. Soft and hard tissue management in implant therapy-part I: surgical concepts. Int J Biomater. 2012;2012:531202.

[10] Zhang W, Zhang S, Liu H, Ren L, Wang Q, Zhang Y. Effects of surface roughening on antibacterial and osteogenic properties of Ti–Cu alloys with different Cu contents. J Mater Sci Technol. 2021;88:158.

[11] Cai DG, Bao MM, Wang XY, Yang L, Qin GW, Wang RX, Chen DF, Zhang EL. Biocorrosion properties of Ti–3Cu alloy in F ion-containing solution and acidic solution and biocompatibility. Rare Met. 2019;38(6):503.

[12] Zhang EL, Fu S, Wang RX, Li HX, Liu HX, Ma ZQ, Liu GK, Zhu CS, Qin GW, Chen DF. Role of Cu element in biomedical metal alloy design. Rare Met. 2019;38(6):476.

[13] Shirai T, Tsuchiya H, Shimizu T, Ohtani K, Zen Y, Tomita K. Prevention of pin tract infection with titanium–copper alloys. J Biomed Mater Res B Appl Biomater. 2009;91(1):373.

[14] Zhang E, Li S, Ren J, Zhang L, Han Y. Effect of extrusion processing on the microstructure, mechanical properties, biocorrosion properties and antibacterial properties of Ti–Cu sintered alloys. Mater Sci Eng C. 2016;69:760.

[15] Ji H, Zhao MC, Xie B, Zhao YC, Yin D, Gao C, Shuai C, Atrens A. Corrosion and antibacterial performance of novel selective-laser-melted (SLMed) Ti-xCu biomedical alloys. J Alloys Compd. 2021;864:158415.

[16] Geetha M, Singh AK, Asokamani R, Gogia AK. Ti based biomaterials, the ultimate choice for orthopaedic implants—a review. Prog Mater Sci. 2009;54(3):397.

[17] Botha SJ. Surface properties and bio-acceptability of Ti$_2$O$_3$ surfaces. Mater Sci Eng A. 1998;243(1):221.

[18] Liu J, Liu J, Attarilar S, Wang C, Tamaddon M, Yang C, Xie K, Yao J, Wang L, Liu C, Tang Y. Nano-modified titanium implant materials: a way toward improved antibacterial properties. Front Bioeng Biotechnol. 2020. https://doi.org/10.3389/fbioe.2020.576969.

[19] Habazaki H, Onodera T, Fushimi K, Konno H, Toyotake K. Spark anodizing of β-Ti alloy for wear-resistant coating. Surf Coat Technol. 2007;201(21):8730.

[20] Zhou H, Xu M, Huang Q, Cai Z, Li W. Anodic behavior of indium in KOH solution. J Appl Electrochem. 2009;39(10):1739.

[21] Arsov LJD, Kormann C, Plieth W. In situ Raman spectra of anodically formed titanium dioxide layers in solutions of H$_2$SO$_4$, KOH, and HNO$_3$. J Electrochem Soc. 2019;138(10):2964.

[22] da Fonseca C, Traverse A, Tadjeddine A, Belo MDC. A characterization of titanium anodic oxides by X-ray absorption spectroscopy and grazing X-ray diffraction. J Electroanal Chem. 1995;388(1):115.

[23] Ohtsuka T, Otsuki T. The aging of the anodic oxide of titanium during potentiostatic condition by ellipsometry. Corros Sci. 2003;45(8):1793.

[24] Xia Z, Nanjo H, Aizawa T, Kanakubo M, Fujimura M, Onagawa J. Growth process of atomically flat anodic films on titanium under potentiostatical electrochemical treatment in H$_2$SO$_4$ solution. Surf Sci. 2007;601(22):5133.

[25] Jin X, Gao L, Liu E, Yu F, Shu X, Wang H. Microstructure, corrosion and tribological and antibacterial properties of Ti–Cu coated stainless steel. J Mech Behav Biomed Mater. 2015;50:23.

[26] Yang Z, Ma C, Wang W, Zhang M, Hao X, Chen S. Fabrication of Cu$_2$O–Ag nanocomposites with enhanced durability and bactericidal activity. J Colloid Interface Sci. 2019;557:156.

[27] Shaikh JS, Pawar RC, Moholkar AV, Kim JH, Patil PS. CuO–PAA hybrid films: chemical synthesis and supercapacitor behavior. Appl Surf Sci. 2011;257(9):4389.

[28] Yan LL, Wang Y, Xiong LB, Li JL, Zhao HR, Wang BQ, Yu Y. Preparation of Cu$_2$O nano array by copper anodic oxidation method and its photocatalytic sterilization performance. Chin J Inorg Chem. 2009;25(11):1960.

[29] Das D, Nath BC, Phukon P, Dolui SK. Synthesis and evaluation of antioxidant and antibacterial behavior of CuO nanoparticles. Colloids Surf B: Biointerfaces. 2013;101:430.

[30] Jin C, Tang Y, Yang FG, Li XL, Xu S, Fan XY, Huang YY, Yang YJ. Cellular toxicity of TiO$_2$ nanoparticles in anatase and rutile crystal phase. Biol Trace Elem Res. 2010;141(1–3):3.

[31] Leprince WY. Study of the initial stages of TiO$_2$ growth on Si wafers by XPS. Surf Coat Technol. 2002;150(2):257.

[32] Yahalom J, Zahavi J. Electrolytic breakdown crystallization of anodic oxide films on A1, Ta and Ti. Electrochim Acta. 1970;15(9):1429.

[33] Shibata T, Zhu YC. The effect of film formation potential on the stochastic processes of pit generation on anodized titanium. Corros Sci. 1994;36(1):153.

[34] Shibata T, Zhu YC. A stochastic analysis of flow velocity effects on the pit generation process on anodized titanium. Corros Sci. 1995;37(5):853.

[35] Wan Y, Wang Y, Liu Z, Qu X, Han B, Bei J, Wang S. Adhesion and proliferation of OCT-1 osteoblast-like cells on micro- and nano-scale topography structured poly(l-lactide). Biomaterials. 2005;26(21):4453.

[36] Kolawole SK, Hai W, Zhang S, Sun Z, Siddiqui MA, Ullah I, Song W, Witte F, Yang K. Preliminary study of microstructure, mechanical properties and corrosion resistance of antibacterial Ti-15Zr-xCu alloy for dental application. J Mater Sci Technol. 2020;50:31.

[37] Habazaki H, Uozumi M, Konno H, Shimizu K, Skeldon P, Thompson GE. Crystallization of anodic titania on titanium and its alloys. Corros Sci. 2003;45(9):2063.

[38] Wang J, Zhang S, Sun Z, Wang H, Ren L, Yang K. Optimization of mechanical property, antibacterial property and corrosion resistance of Ti–Cu alloy for dental implant. J Mater Sci Technol. 2019;35(10):2336.

[39] Chen M, Yang L, Zhang L, Han Y, Lu Z, Qin GW, Zhang EL. Effect of nano/micro-Ag compound particles on the bio-corrosion, antibacterial properties and cell biocompatibility of Ti-Ag alloys. Mater Sci Eng C. 2017;75:906.

[40] Shi AQ, Zhu C, Fu S, Wang RX, Qin GW, Chen DF, Zhang EL. What controls the antibacterial activity of Ti–Ag alloy, Ag ion or Ti$_2$Ag particles? Mater Sci Eng: C. 2020;109:110548.

[41] Cao GJ, Cui B, Wang WQ, Tang GZ, Feng YC, Wang LP. Fabrication and photodegradation properties of TiO$_2$ nanotubes on porous Ti by anodization. Trans Nonferrous Met Soc China. 2014;24(8):2581.

[42] Ren G, Hu D, Cheng EWC, Vargas-Reus MA, Reip P, Allaker RP. Characterisation of copper oxide nanoparticles for antimicrobial applications. Int J Antimicrob Agents. 2009;33(6):587.

[43] Karuppannan SK, Ramalingam R, Khalith SM, Dowlath MJ, Raiyaan GD, Arunachalam KD. Characterization, antibacterial and photocatalytic evaluation of green synthesized copper oxide nanoparticles. Biocatal Agric Biotechnol. 2021;31:101904.

[44] Katwal R, Kaur H, Sharma G, Naushad M, Pathania D. Electrochemical synthesized copper oxide nanoparticles for enhanced photocatalytic and antimicrobial activity. J Ind Eng Chem. 2015;31:173.

[45] Lee YJ, Kim S, Park SD, Park H, Huh YD. Morphology-dependent antibacterial activities of Cu$_2$O. Mater Lett. 2011;65(5):818.

[46] Zhang JT, Liu JF, Peng Q, Wang X, Li YD. Nearly monodisperse Cu$_2$O and CuO nanospheres: preparation and applications for sensitive gas sensors. Chem Mater. 2006;37(17):867.

[47] Ren J, Wang W, Sun S, Zhang L, Wang L, Chang J. Crystallography facet-dependent antibacterial activity: the case of Cu$_2$O. Ind Eng Chem Res. 2011;50(17):10366.

[48] Jung HY, Seo Y, Park H, Huh YD. Morphology-controlled synthesis of octahedral-to-rhombic dodecahedral Cu$_2$O

microcrystals and shape-dependent antibacterial activities. Bull Korean Chem Soc. 2015;36(7):1828.

[49] He LJ, Hao JC, Dai L, Zeng RC, Li SQ. Layer-by-layer assembly of gentamicin-based antibacterial multilayers on Ti alloy. Mater Lett. 2020;261:127001.

[50] Burghardt I, Luthen F, Prinz C, Kreikemeyer B, Zietz C, Neumann HG, Rychly J. A dual function of copper in designing regenerative implants. Biomaterials. 2015;44:36.

[51] Siddiqui MA, Ullah I, Liu H, Zhang S, Ren L, Yang K. Preliminary study of adsorption behavior of bovine serum albumin (BSA) protein and its effect on antibacterial and corrosion property of Ti–3Cu alloy. J Mater Sci Technol. 2021;80:117.

[52] Kasemo B. Biocompatibility of titanium implants: surface science aspects. J Prosthet Dent. 1983;49(6):832.

[53] Feng B, Weng J, Yang BC, Qu SX, Zhang XD. Characterization of surface oxide films on titanium and adhesion of osteoblast. Biomaterials. 2003;24(25):4663.

[54] Xing J, Xia Z, Hu J, Zhang Y, Zhong L. Time dependence of growth and crystallization of anodic titanium oxide films in potentiostatic mode. Corros Sci. 2013;75:212.

[55] Roughead ZK, Lukaski HC. Inadequate copper intake reduces serum insulin-like growth factor -I and bone strength in growing rats fed graded amounts of copper and zinc. J Nutr. 2003;133(2):442.

[56] Li S, Xie H, Li S, Kang YJ. Copper stimulates growth of human umbilical vein endothelial cells in a vascular endothelial growth factor-independent pathway. Exp Biol Med (Maywood). 2012;237(1):77.

[57] Gérard C, Bordeleau LJ, Barralet J, Doillon CJ. The stimulation of angiogenesis and collagen deposition by copper. Biomaterials. 2010;31(5):824.

[58] Zhang Y, Wang X, Ma Z, Bai B, Liu J, Yang L, Qin GW, Zhang EL. A potential strategy for in-stent restenosis: inhibition of migration and proliferation of vascular smooth muscle cells by Cu ion. Mater Sci Eng: C. 2020;115:111090.